Experimental electron heat diffusion in ECH plasmas of the TJ-II stellarator

2007 Nucl. Fusion 47 1367

(http://iopscience.iop.org/0029-5515/47/9/039)

IOP Publishing and International Atomic Energy Agency Nuclear Fusion
Nucl. Fusion **47** (2007) 1367–1375 doi:10.1088/0029-5515/47/9/039

Experimental electron heat diffusion in ECH plasmas of the TJ-II stellarator

V.I. Vargas, D. López-Bruna, J. Herranz, F. Castejón and the TJ-II Team

Laboratorio Nacional de Fusión por Confinamiento Magnético Asociación Euratom-CIEMAT, Madrid, Spain

Received 14 December 2006, accepted for publication 31 July 2007
Published 3 September 2007
Online at stacks.iop.org/NF/47/1367

Abstract
Interpretative transport has been used to revisit the global scalings of TJ-II plasmas with electron cyclotron resonance heating (ECH), from a local perspective. Density, rotational transform and ECH power scans were analysed based mainly upon Thomson scattering data (electron density and temperature) in steady state discharges. The thermal diffusivity χ_e is estimated assuming pure diffusion and negligible convective heat fluxes in a set of 201 discharges. The density scan indicates that for normalized minor radii $\rho \lesssim 0.4$ there is no significant change of χ_e with density in the range studied ($0.5 < \bar{n}_e(10^{19}\,\mathrm{m}^{-3}) < 0.9$), while in the density gradient region, χ_e decreases with line density. In the rotational transform scan, there is an overall tendency of χ_e to decrease with increasing rotational transform, but we also find that the presence of a low order rational value of the rotational transform is accompanied by a local *lowering* of χ_e. Finally, in the ECH power scan, χ_e is found to have an overall increment in $0.2 < \rho < 0.6$ when Q_{ECH} increases from 200 to 400 kW, although it is less significant in the density gradient region.

PACS numbers: 52.25.Fi, 52.55.−s, 52.55.Hc

1. Introduction

Some of the main trends of the ISS04 global stellarator scaling for the energy confinement time [1] were already observed in the early times of medium-sized machines. For instance, the energy confinement time degradation/improvement with power/density $\tau_E \sim P^{-0.61}\bar{n}^{0.54}$ was observed to be almost identical in the Heliotron-E [2]. Another commonly accepted result was the distinction between a plausibly neoclassical behaviour in the innermost plasma but an anomalously high transport towards the edge (see, e.g. [3]). Actually, assuming that the anomaly should originate from turbulent transport, some groups devoted themselves to identifying the dominant instability [4]. The upgrading of plasma diagnostics, along with an increasingly large data set of discharges, has allowed obtaining a rather complete notion about which are the common leading parameters for confinement in stellarators independently of confining device. Thus, the machine size, the magnetic field, the heating power, the plasma density and the rotational transform contribute significantly to explain stellarator confinement times for essentially all kinds of device. Still, there is room for improvement because a correction factor coming from the particular magnetic configuration design must be taken into account [1].

The fact that TJ-II data adjust well to the ISS04 scaling is an indication that, despite the somewhat peculiar heliac configuration, TJ-II plasmas share the main transport physics of current-less plasmas for magnetic fusion. These trends were summarized in a previous work on electron cyclotron resonance heating (ECH) plasmas of the TJ-II, where density ($\bar{n}_e$), rotational transform (ι) and ECH power scans were studied [5] from the perspective of *global* confinement. As a next step, here we proceed to show results from *local* power balance analysis in similar scans. Not only are we interested in knowing where in the plasma the changes in confinement are substantiated: the TJ-II should exploit its main operational virtue, the accurate control of vacuum rotational transform values, to contribute to the understanding of rotational transform effects in confinement. In this respect, most of the work done so far has focused on the effects of the edge rotational transform ι_a on confinement, notably by the Wendelstein VII-AS group [6]. Even so, the role of low order rational surfaces on confinement is still not clear. On the one hand, the access to improved confinement in stellarators was soon related to the presence of such low order rationals in the plasma edge region [7, 8], something that is commonly interpreted in terms of 'separatrix' effects. On the other hand, quite an effort has been devoted to *avoiding* low order rationals of ι, especially in low shear machines, using every available mechanism of current drive control to keep the ι-profile away from low order rationals. The TJ-II device may well clarify the effect of such low order rationals. It is a high ι machine with low shear, and the experience indicates that the lowest order rationals do not necessarily deteriorate confinement when they are located in the bulk plasma. Moreover, it has been found that a small amount of shear ($|\hat{s}| = |-(\rho/\iota)(\mathrm{d}\iota/\mathrm{d}\rho)| \gtrsim 0.1$,

where ρ is a normalized flux-surface label) not only allows including the lowest order rationals inside the plasma, but also the transport in the density gradient region decreases roughly obeying the shear strength [9]. Here, we perform a scan to follow some vacuum low order rationals through the plasma, in order to search for the local effect of these rationals in close-to-vacuum shear conditions. This is but exploiting a natural advantage of stellarators, as is the external control of the confining magnetic field, to learn about its possible effects.

In the following sections we expose the results obtained after performing interpretative transport analysis on several scans of TJ-II discharges under ECH conditions. Our results are therefore limited to the range of attained *stationary* densities, $\bar{n}_e \lesssim 0.9 \times 10^{19}\,\mathrm{m}^{-3}$ below ECH cut-off and, for the given maximum power, to low β. As expected, most of our results are in concordance with studies made at the CHS [10, 11], LHD [12] and W7-AS [6, 13, 14] devices. The general experimental setup that corresponds to this work is briefly described in section 2. The transport analysis and the details of the scans are presented in section 3, while the results, along with some discussion, are presented in section 4. The paper ends with a summary in section 5.

2. Experimental setup

The plasmas presented here were obtained in the 4-period, low magnetic shear, TJ-II stellarator device [15] (major radius $R = 1.5\,\mathrm{m}$, average minor radius $a \approx 0.2\,\mathrm{m}$, magnetic field strength $B_0 \approx 1.0\,\mathrm{T}$). It was designed to explore a wide range of rotational transforms ($0.9 \leqslant \iota = \iota/2\pi \leqslant 2.2$) in low shear configurations. The TJ-II is a limiter machine with its last closed flux surface (LCFS) defined by either its two movable graphite poloidal limiters or by its helical one (i.e. the side of the vacuum chamber that encapsulates the central conductor). Plasmas are created and maintained by ECH ($f = 53.2\,\mathrm{GHz}$ tuned to 2nd harmonic, $Q_{\mathrm{ECH}} \leqslant 500\,\mathrm{kW}$ (2 gyrotrons), X-mode polarization, pulse duration $t_{\mathrm{ECH}} \leqslant 300\,\mathrm{ms}$) with hydrogen as the main plasma species. The last mirror of each of the quasi-optical microwave transmission lines is located inside the vacuum vessel and allows for current drive (ECCD), although for the present experiments ECCD was avoided. The power density in the deposition zone is $\approx 15\,\mathrm{W\,cm}^{-3}$.

In order to achieve reproducible and controlled discharges for ECH power injection, both gas control and wall conditioning techniques are implemented. In the experiments reported here, the inner wall was boronized and very low Z_{eff} values were inferred from radiation diagnostics [16]. Typically, He glow discharge cleaning is performed prior to device operation.

Radial electron temperature and density profiles are obtained using a single-shot, high resolution (2.5 mm), Thomson scattering (TS) system [17]. The temporal evolution of the electron temperature profile is measured using a 16-channel, absolutely calibrated, electron cyclotron emission (ECE) radiometer [18]. For the ECE data in this paper only the emission coming from the plasma centre to the edge on the high-field side was used. The sampling frequency of the channels is 20 kHz and the spatial resolution is 1 cm. Next, the line-averaged electron density evolution is measured by a fast 2-channel microwave interferometer. Furthermore, the central ion temperature is obtained by a charge exchange neutral particle analyser [19], while the total plasma radiation is monitored using bolometer arrays [20]. Finally, a reflectometer (RF) system [21] provides the radial electron density profile at the edge.

The plasmas selected for this study had the mobile limiter at/outside the LCFS and were stationary at the time of the TS firing. In all cases the plasmas have a characteristic bean shaped cross-section. A sample of 201 steady state discharges corresponding to different campaigns has been selected. For consistency, a fair number of them coincide with the scans of [5]. Typical numbers for these discharges are: line-averaged density $< 0.9 \times 10^{19}\,\mathrm{m}^{-3}$; central electron and ion temperatures $\leqslant 1.2\,\mathrm{keV}$ and $\sim 0.09\,\mathrm{keV}$, respectively; thermal energy content $\leqslant 0.8\,\mathrm{kJ}$; net plasma current (in absolute value) $< 0.5\,\mathrm{kA}$ and energy confinement time $\leqslant 4\,\mathrm{ms}$.

In this study, smoothed TS T_e profiles were constructed using the algorithm:

$$R_i = \frac{1}{w}\sum_{j=0}^{w-1} A_{i+j-w/2} \qquad i = \frac{(w-1)}{2}, \ldots, N - \frac{(w+1)}{2}, \tag{1}$$

where A is the array to be smoothed (T_e and n_e profiles), R_i stands for the i-position in the smoothed profile A; N (measured spatial points) is the number of elements in the profile A, and w represents the width of the smoothing window. The $w = 0.05 \times N$ criteria, as given by [22], was used. This low degree of smoothing (5%) allows removal of the random or small-scaled structures but it keeps the main shape of the measured profile in the region of interest. These profiles were extended to the edge using a parabolic function with an edge value of 20 eV and compared with ECE radiometer data, which are in agreement with TS data for these plasma conditions [18]. n_e profiles from the TS are completed with edge data from the AM reflectometry diagnostic (the TS data are not accurate at low densities due to unfavourable signal to noise ratios). However, AM reflectometry data were unavailable for some discharges so the corresponding TS profiles were extended to the edge using a parabolic function. Finally, line density integrals were performed to ensure that the integral values for the reconstructed density profiles matched the experimental line densities measured with interferometry techniques.

As shown in figure 1, TJ-II ECH density profiles n_e are hollow, with the density gradient region starting at a normalized radius $\rho \approx 0.6$, while electron temperature profiles have central peaked values of about 0.8–1.2 keV. Although these TS electron density and temperature profiles show structures typical of TJ-II ECH discharges [23] we will perform transport analysis on smoothed profiles.

In the case of T_i, charge exchange data were available for only a limited number of discharges. Nonetheless, T_i profiles in TJ-II ECH shots are flat with values close to 90 eV [24]. Hence a 90 eV flat profile, dropping to 12 eV at the boundary, is used for all discharges analysed.

3. Transport analysis

Interpretative analysis has been done to estimate local changes in the heat diffusion $\chi_e(\rho)$ as density, rotational transform and

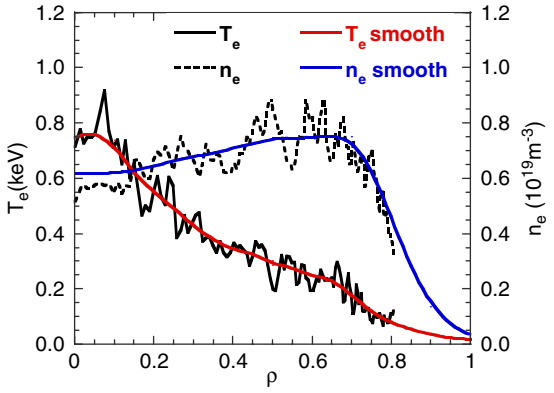

Figure 1. Electron density (- - - -) and temperature (——) profiles measured by the TS diagnostic in a typical TJ-II ECH discharge. The smoothed profiles used for the analysis are superimposed.

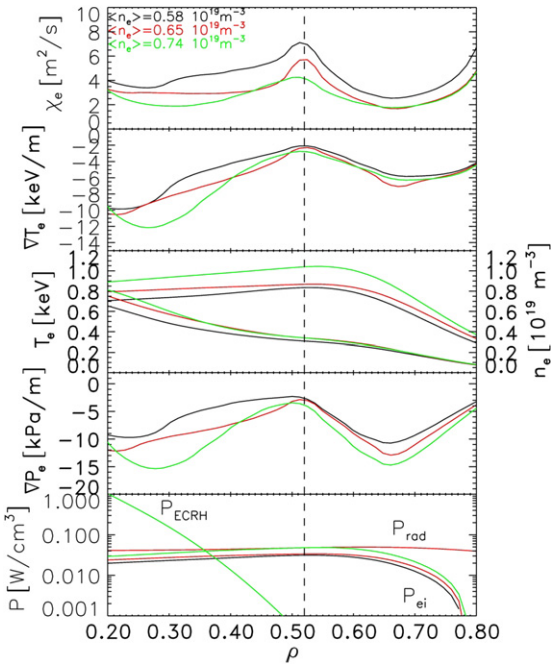

Figure 2. From top to bottom: electron heat diffusivity, electron temperature gradient, electron temperature, electron density, pressure gradient and power density profiles ($P_{\rm ECH}$ is the power transferred to the electron by ECH, $P_{\rm rad}$ is the radiated power, $P_{\rm ei}$ is the power transferred to the ions by collisions) for three discharges: #9693 ($\bar{n}_{\rm e} = 0.58 \times 10^{19}$ m^{-3}; black), #10091 ($\bar{n}_{\rm e} = 0.65 \times 10^{19}$ m^{-3}; red) and #10089 ($\bar{n}_{\rm e} = 0.74 \times 10^{19}$ m^{-3}; green).

ECH power are changed. This analysis is primarily based on the experimental profiles of $n_{\rm e}$ and $T_{\rm e}$. An example of the results of this analysis is shown in figure 2 for three discharges with differing line-averaged electron densities in the density scan experiments. The heating source is taken to be a constant Gaussian-shaped profile. This is consistent with the measured power deposition profile obtained from modulation experiments [25] and we consider it to be centred with a fixed width $\Delta\rho = 0.2$. It has been checked that the microwave absorption signals are similar for all discharges in the density and rotational transform scans, so we assume the same deposited heating power. Instead of the corresponding nominal value ($Q_{\rm ECH} = 400$ kW), we take the same precautions as in [5] and reduce it by 40% to take into account several known losses in the path from the gyrotrons to the resonant plasma [26]. Radiation losses can amount to roughly 10% in these plasmas and will not be included in this work because the corresponding experimental information was not available for all the discharges in the scans. However, in smaller sets we checked that the inclusion of this information does not alter the results in a significant way. The collisional electron–ion energy transfer can also be neglected (see figure 2) but it has been included in the analysis. All the analysis was performed with the ASTRA shell [27] after imposing TJ-II flux-surface averages of the metrics to estimate gradients and volume integrals properly. An effective electron heat diffusivity is obtained as usual:

$$\chi_{\rm e}(\rho) = -\frac{Q_{\rm e}^{\rm T}(\rho)}{n_{\rm e}(\rho)\nabla T_{\rm e}(\rho)G(\rho)}, \qquad (2)$$

where $Q_{\rm e}^{\rm T} = \int^{\rho} P_{\rm e}^{\rm T} {\rm d}V$ is the total power deposition inside the flux surface labelled ρ, and the total power density to the electrons only includes, as mentioned, the ECH and electron–ion heat exchange, $P_{\rm e}^{\rm T} = P_{\rm ECH} - P_{\rm ei}$. The geometry enters through $G = \frac{\partial V}{\partial \rho}\left\langle(\nabla\rho)^2\right\rangle$ where V is the plasma volume and the angular brackets represent the flux-surface average.

The analysis has been reduced to the plasma region $0.2 < \rho < 0.8$ for the following reasons. Near the magnetic axis, not only the features of the TS profiles make the zero-gradient zone shift slightly from $\rho = 0$ after smoothing, but also the ECH deposition is worse determined. Therefore, and given the fact that $\chi_{\rm e}$ from the electron energy balance analysis in the central region depends sensitively on the ECH power deposition profile, we reject any results near the magnetic axis. Likewise, any heat loss due to escaping supra-thermal particles in the ECH sector of the TJ-II [28] can be ascribed to the ECH integrated power, which would not affect our effective $\chi_{\rm e}$ except for a small offset. At the plasma edge, $\rho > 0.8$, the heat transport probably has significant contributions from convection (magnetic field ripple losses) or other terms related to the proximity of the wall. Our experience is that a convective term in the heat balance does not change substantially the results in the bulk plasma unless we assume an unreasonably large net radial velocity of thermal particles. However, this could be a contribution to take into account in the plasma periphery. Additionally, $\nabla T_{\rm e}$ is quite small near the edge and has larger error bars than inside, which propagate into largely undetermined values for $\chi_{\rm e}$ from equation (2). Therefore, we give little credit to the results outside $\rho \approx 0.8$ while our effective $\chi_{\rm e}$ in equation (2) is probably a reasonable estimate of the heat diffusion according to the standard picture of transport.

As a general rule, discharges grouped by small density ranges, vacuum rotational transform at plasma edge and heating power were used to obtain averages of $\chi_{\rm e}(\rho)$ and the dispersion as standard deviation within the groups. In more detail we have the following scans:

Density scan. We used 78 shots with line-averaged densities in the range 0.5×10^{19} m^{-3} $< \bar{n}_{\rm e} < 0.9 \times 10^{19}$ m^{-3} in a typical magnetic configuration of the TJ-II, where $\iota(a) = 1.65$,

$\iota(0) = 1.55$ and $a = 0.2$ m (plasma volume 1.1 m^3). For this configuration, the vacuum $\iota = 8/5$ resonance is in $\rho = 0.77$. From all this set, nine groups of approximately nine discharges each were formed. The maximum differences allowed within a group were $\delta\bar{n}_e = 0.07 \times 10^{19}$ m^{-3}. After finding the corresponding nine average profiles of χ_e, we found it appropriate to perform a power-law fit $\chi_e(\rho) \propto \bar{n}^{\alpha(\rho)}$ over selected radii to check for the significance of the ρ-dependent fitting coefficients, $\alpha(\rho)$.

Rotational transform scan. Eighty nine shots were used with edge values in the interval $1.4 \leqslant \iota_a \leqslant 2.2$. The line-averaged densities range between 0.6×10^{19} m^{-3} and 0.7×10^{19} m^{-3} and the plasma volume between 0.6 m^3 and 1.1 m^3. As a first step, 14 magnetic configurations were taken to make an analysis over this wide range of ι_a. After that, a pattern in $\chi_e(\rho)$ seemed to appear in relation with the position of the low order rationals. Therefore, we next performed a fine magnetic configuration scan aimed at following the effects on χ_e of moving low order rationals through the confinement region. These scans were performed at constant plasma volume (1.1 m^3) ensuring that two consecutive rationals, $\mathsf{n/m} = 8/5$ and $\mathsf{n/m} = 5/3$ were moved inwards on a shot to shot basis in stationary conditions. Here m and n are the poloidal and toroidal numbers, respectively. Thirty six discharges for this fine rational surface sweep were used, with edge values $1.65 \leqslant \iota_a \leqslant 1.75$ in 13 magnetic configurations. The plasma line-averaged density ranged also between 0.6×10^{19} m^{-3} and 0.7×10^{19} m^{-3}. The corresponding vacuum ι profiles are shown in figure 3, where we can see how the position of the two selected low order magnetic resonances is changed from one discharge to the next. The main control variable is the current fed into the helical windings, I_h. It is also worth noting that the metrics of these configurations (mainly $\mathrm{d}V/\mathrm{d}\rho$, $\langle|\nabla\rho|\rangle$ and the position of the magnetic axis) are identical for practical purposes in the whole scan. Therefore, the heat deposition, the evaluation of flux-surface averaged gradients and the mapping of TS data to ρ should not be affecting the evaluation of χ_e. Moreover, the effective magnetic field ripple, a magnitude related to the proximity of the confining volume to the toroidal field coils, depends in the TJ-II almost exclusively on the plasma volume (especially if, as is the case, the shape of the plasma cross-section does not change substantially). Therefore, the fine scan in rotational transform is performed at constant magnetic ripple.

ECH power scan. Finally, 34 shots were used for the ECH power scan in on-axis heating conditions. Due to difficulties in evaluating the heating power, a reliable data set could only be obtained for three nominal power values: 200 kW, 300 kW and 400 kW. Densities were constrained to lie between 0.6×10^{19} m^{-3} and 0.7×10^{19} m^{-3} in the same configuration as the density scan (see above). The data consists of 12 discharges at $Q_{ECH} = 200$ kW; 4 discharges with $Q_{ECH} = 300$ kW and 18 discharges with $Q_{ECH} = 400$ kW. Let us recall that to estimate χ_e we have reduced the nominal power so that the values taken for the analysis are $Q_{ECH} = 120$ kW, $Q_{ECH} = 180$ kW and $Q_{ECH} = 240$ kW, respectively. Given the narrow heat deposition zone, this is simply a constant factor for the χ_e profiles.

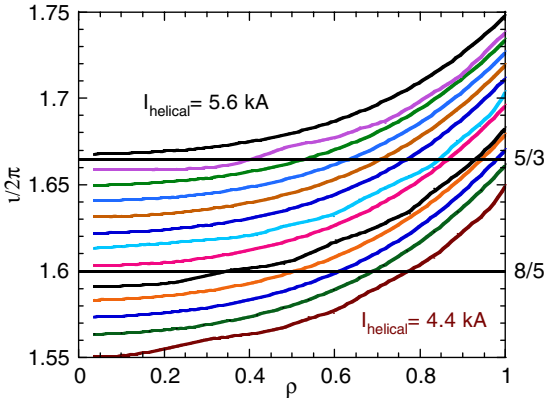

Figure 3. Vacuum rotational transform profiles for a configuration scan where the $\mathsf{n/m} = 8/5$ and $\mathsf{n/m} = 5/3$ values of ι are moved along the plasma minor radius.

4. Experimental results

4.1. Density scan

ECH plasmas of the TJ-II are quite collisionless and the distribution of magnetic traps in the confining volume is easily felt by the particles. In general, these plasmas have large values of χ_e (roughly between 1 m^2 s^{-1} and 10 m^2 s^{-1}) as expected from collisional transport estimates. Still, the density effect in the electron heat diffusion can be clearly detected. From the density scan, we can see that the local heat diffusivities in the density gradient region (roughly the outer half of the plasma, see figure 2) decrease with line average density. Figures 4(*a*) and 4(*b*) show the dependence of χ_e with $\bar{n}_e$ for different values of ρ. The dots represent the average values of χ_e for the different groups of discharges with similar density; the vertical and horizontal bars correspond to the standard deviations of χ_e and $\bar{n}_e$, respectively. A power-law fit is suited to capture the local variation at each ρ in the density gradient region and the corresponding fits indicate that χ_e decreases significantly as $\bar{n}_e$ increases. This decrement is found to be due to the increasing values of n_e while the electron temperature gradients remain constant (see equation (2)) as the line density increases. A different result is found inside $\rho \approx 0.4$; the power-law fit does not yield exponents significantly different from zero, i.e. the local fits consist of a constant diffusivity for all the densities in the scan although with large uncertainty ($\lesssim$50%). This kind of fitting for a fixed radius has been done in the entire range $0.2 \leqslant \rho \leqslant 0.8$ every $\Delta\rho = 0.05$, although figure 4 only shows a few positions for clarity.

A synopsis of our estimates can be obtained from the four panels of figure 5. In figure 5(*a*) we show χ_e in the range $0.2 < \rho < 0.8$ as a function of line average density. The map has been obtained after doing a simple linear interpolation of the data set. Figure 5(*b*) represents the standard deviation that corresponds to figure 5(*a*). We can see that the largest values of the standard deviation are found in the inner half of the plasma but the outer side, on the contrary, is characterized by smaller statistical dispersion. Taking this into account and the fits for every radial position (like those of figures 4) we can draw a 'clean' map that shows the values obtained from the fitting functions (figure 5(*c*)). As mentioned, we do not obtain statistically significant changes inside $\rho = 0.4$ while

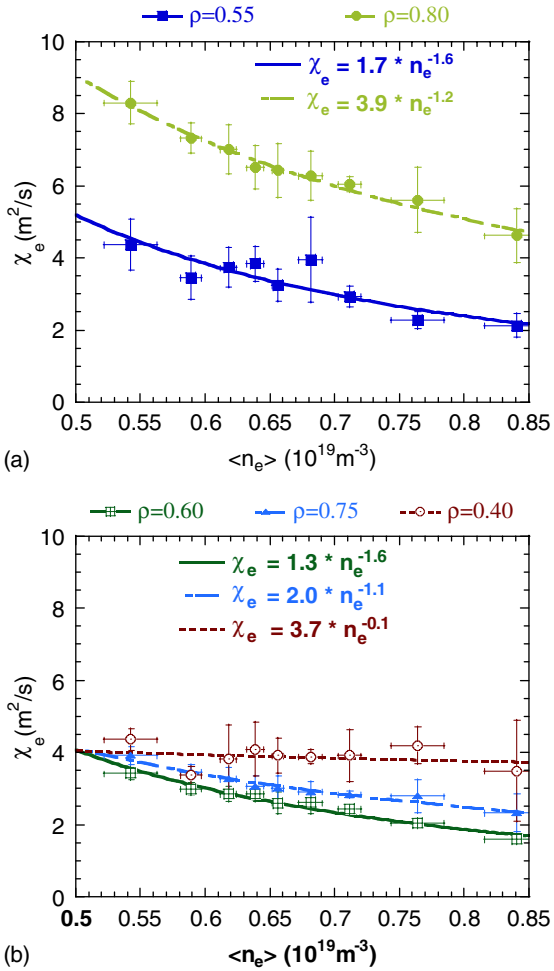

Figure 4. Experimental values of χ_e at: (a) $\rho = 0.55$ and $\rho = 0.80$ and (*b*) $\rho = 0.40$, $\rho = 0.60$ and $\rho = 0.75$ as a function of line average density. The data points are obtained from average to small density ranges in the density scan. The bars represent standard deviation and power-law fits are shown.

the decline of χ_e outside $\rho \approx 0.5$ is quite evident. Finally, figure 5(*d*) represents the absolute error that is obtained from error propagation in the power-law fits.

A clear feature in figures 5(*a*) and (*c*) is the local maximum of χ_e found around $\rho = 0.5$ for low densities that fades out above $\bar{n}_e \approx 0.7 \times 10^{19}$ m^{-3}. We have checked that this maximum does not come from the density profile, which has a 'shoulder' in the same position in these typically hollow profiles of ECH plasmas, but from a flattening of the T_e profile (see figure 2). Noting that the errors are also larger in that region, we studied a group of steady state discharges to see whether the variability comes from fluctuations of ∇T_e during the discharge. The time evolution of ∇T_e was studied using the ECE diagnostic (T_e^{ECE}) for 64 discharges belonging to the density scan. At constant $\bar{n}_e$, T_e^{ECE} was collected for ± 10 ms around the time in which the firing of the TS diagnostic occurs. The result is that the time variation of ∇T_e in $\rho \approx 0.5$ within a discharge cannot explain the statistical dispersion among discharges. It is likely that the smoothing of TS data is sensitive to the well-known spatial structures of the TS T_e profile [23], but the coincidence of a large variability of χ_e (or of ∇T_e from TS) and a large χ_e (or small ∇T_e) in this region suggests that there is a common physical origin. We shall come back to this when we discuss the rotational transform scan.

Another clear result is that χ_e presents a local minimum in the density gradient region that is deeper for larger $\bar{n}_e$. The result is consistent with the favourable scaling of τ_E with density for the TJ-II [5] and agrees with known results from other machines (e.g. [13]).

4.2. Rotational transform scan

The magnetic configuration, or ι scan, has revealed that a global scaling may be affected by the presence of low order rationals because they affect χ_e locally. Throughout this paragraph we shall consider low order rational meaning poloidal number $2 < m \leqslant 6$. In figure 6(*a*) we plot χ_e at $\rho = 0.75$ as a function of the corresponding local value of ι for a set of 14 magnetic configurations in steady state plasmas with approximately the same line density. The dots represent averaged values (see section 3), the vertical bars indicate standard deviation and several low order rational values are marked with vertical lines. A power law with a small but significant negative exponent is found to be valid for $\rho > 0.60$, i.e. roughly in the density gradient region [29]. Even though in figure 6(*a*) we include many configurations without paying attention to the plasma volume, it is apparent a general tendency of χ_e to decrease with increasing ι, as indicated by the power-law fit, which agrees with the notion of a beneficial effect of ι on confinement found particularly in the TJ-II [5] but also in the general ISS04 scaling [1]. In addition, it can be noticed that the values of χ_e when a low order rational of ι is coincident in $\rho = 0.75$ (solid vertical lines in figure 6(*a*)) are generally found below the main trend and conversely: when no low order rational is present, χ_e seems to stay above the fit. In figure 6(*b*) we select the subset of nine magnetic configurations that share a similar volume to plot the values of χ_e for two different radii: $\rho = 0.75$ as before and $\rho = 0.55$, where we can observe that a power-law fit is not significant. In this case we cannot label the abscissa with the local values of ι so we use ι_a instead. As a rule of thumb, a constant volume in the configuration space of the TJ-II can be obtained when the sum of the first two numbers in the configuration labels (indicated also in figure 6(*b*)) is constant. Such numbers respond to the plasma currents (hundreds of A) respectively, in the circular and helical windings of the central conductor. It is interesting to observe that not only the same bumpiness is found in $\chi_e(\rho = 0.55)$, but also that it seems to be 'out of phase' with the bumps for $\rho = 0.75$ independently of whether or not there is a significant power-law fit. The curves are drawn to guide the eye. Looking at the magnetic configurations with more detail (not shown) led us to suspect that a structure in χ_e is actually present as a consequence of the ι-profile, being the low order rationals responsible for a local lowering of χ_e.

The scan in figure 6(*b*) is too broad in ι to draw clear conclusions on the suggested effect of the local ι. The reason is that the displacement of a given low order rational in minor radius when we move from one configuration to the next is too large. Even if we normally see a local coincidence between lower χ_e and the presence of a low order rational, a better proof of the effect should be obtained if we can *follow* closely the

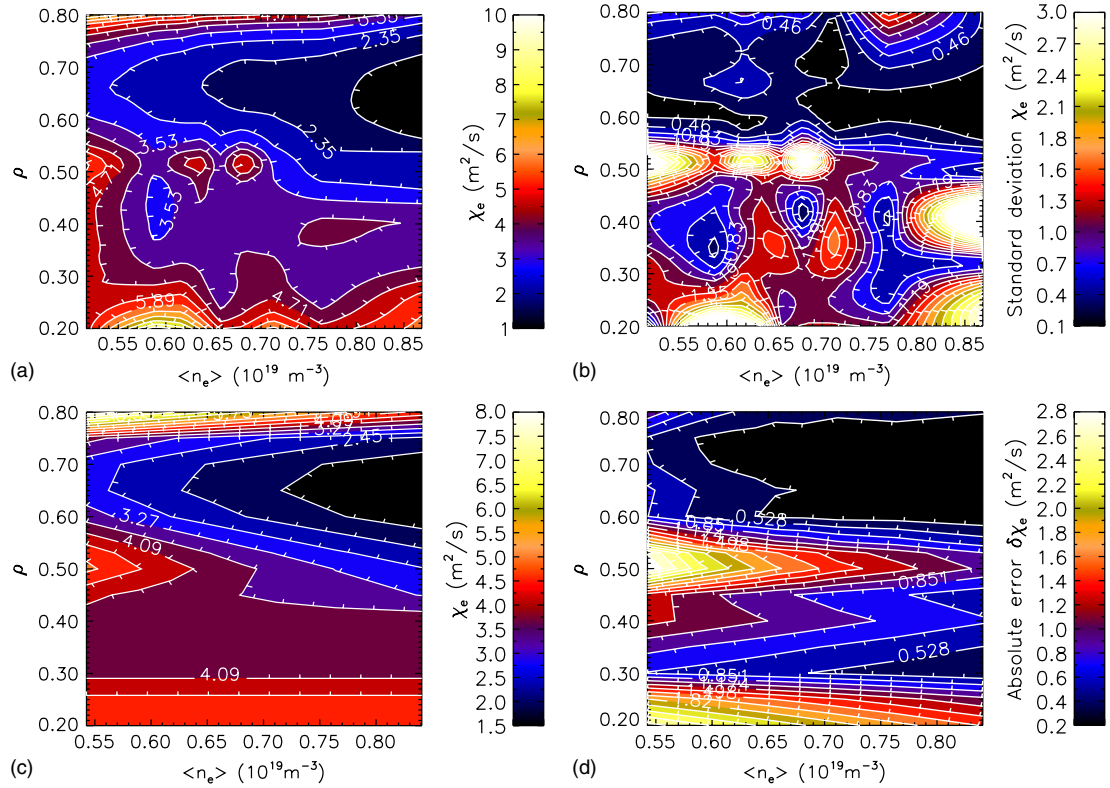

Figure 5. Contour maps of (*a*) $\chi_e(\rho)$ in the radial interval $0.2 \leqslant \rho \leqslant 0.8$ for different line average densities; (*b*) standard deviation values for the profiles of 5(*a*); (*c*) χ_e obtained from the power-law fits $\chi_e = \chi_e(\bar{n}_e)$ in selected radii and (*d*) standard error from the fitting parameters of 5(*c*).

suspected pattern continuously through the radial positions. A new experiment was designed with this purpose, which is the fine scan of figure 3 and whose extension in ι can be compared with the broad scan by noting the square mark at the top of figure 6(*b*). The results for χ_e are shown again in the manner of contour maps (figure 7(*a*)), except that now we plot the profiles as themselves, without performing any interpolation. Therefore, we label the configurations with the main experimental control variable, I_h, and show the data with the accuracy in the I_h dimension as given by the configuration scan, 0.1 kA. The figure is intended to show that there is actually a pattern of 'furrows' and 'ridges' whose direction follows roughly the path of rationals through the minor radius as I_h increases (i.e. as the rationals move inwards). To stress this, we have also drawn with white lines the path followed by the vacuum $\iota = 8/5$ (left) and $\iota = 5/3$ (right) in the (ρ, I_h) plane. In figure 7, ρ has been extended to 0.9 in order to emphasize the effect of the low order rational on χ_e despite the errors being large in the outermost region. Figure 7(*b*) shows the standard deviation values that correspond to the profiles in figure 7(*a*). Note, at $I_h = 5.2$ the standard deviation vanishes as there is only one discharge for that value. We can observe, as we did in the density scan (figure 5(*a*)), that the largest errors are associated with the largest diffusivities and conversely. Observe also that the configuration that corresponds to the density scan is the leftmost one in figure 7(*a*) ($I_h = 4.4$ kA). The densities in this fine ι-scan are around 0.65×10^{19} m^{-3} and we have now reasons to suspect that the furrow seen in the density scan is a consequence of the presence of the $\iota = 8/5$ in $\rho = 0.77$, from which we may expect the same furrow in other configurations deepening as the line density is increased, but in different radial positions corresponding to a different position of the low order rational. This and other aspects will be explored with further experiments.

One is naturally tempted to perform a linear interpolation following the lines that would correspond in figure 7(*a*) to the smallest directional derivatives of χ_e in the (ρ, I_h) plane. In other words, we would like to uncover the levels of iso-diffusivity. Since the data are not dense enough in the I_h dimension, we perform a linear interpolation in a rotated mesh: figure 8 is obtained from the same data but we have interpolated linearly along lines with the same slope as the path of the 8/5 low order rational in the range $0.6 < \rho < 0.8$. The choice of range is not completely arbitrary: the net plasma currents in the complete set are always around -0.5 kA and the largest current densities are expected to be largest inside $\rho \approx 0.5$ due to the bootstrap current contribution. Since these are very low β plasmas, such contribution is expected to be small and the vacuum rotational transform should be quite close to the vacuum one, at least in the outer half of the plasma. Therefore we can reasonably trust the paths drawn for $\rho > 0.5$ in figures 7 and 8 for the low order rationals despite being correspondent to vacuum configurations, and in this way our linear interpolation can be told to be performed along the lines drawn by the low order rationals *in the configuration with plasma*. In figure 8 we have also drawn, with dashed lines, the path followed by the next lowest order rational values of the vacuum ι in the range between 8/5 and 5/3, i.e. the 13/8 (left) and 18/11 (right) rationals. The impression from this figure is that not only the low order rationals retain heat fluxes where

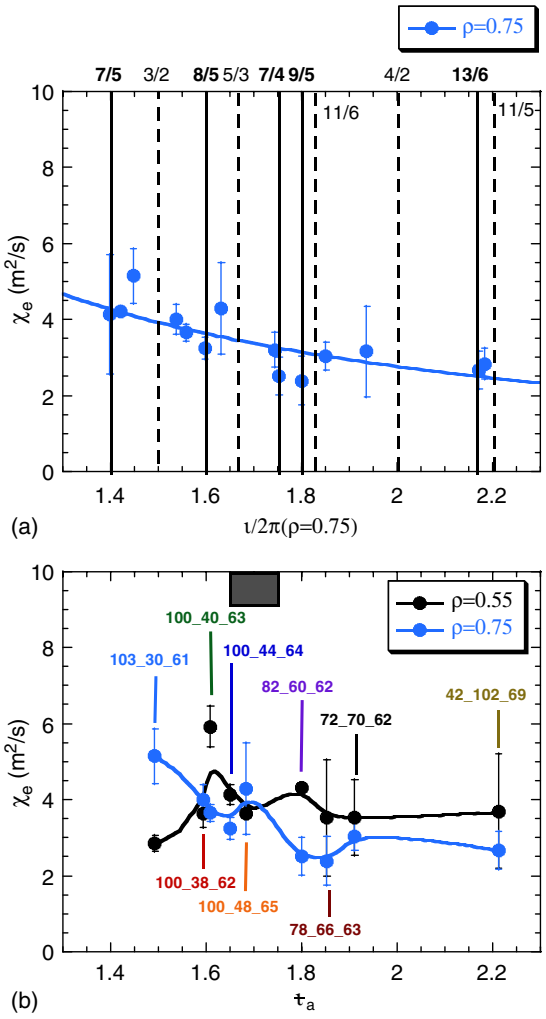

Figure 6. (*a*) Configuration-averaged χ_e at $\rho = 0.75$ as a function of the local ι (●) and power-law fit (——) for a set of 14 magnetic configurations. (*b*) χ_e at $\rho = 0.75$ (light blue dots) and $\rho = 0.55$ (black dots) as a function of the edge rotational transform for the subset of (*a*) with similar volume. The bars represent standard deviation.

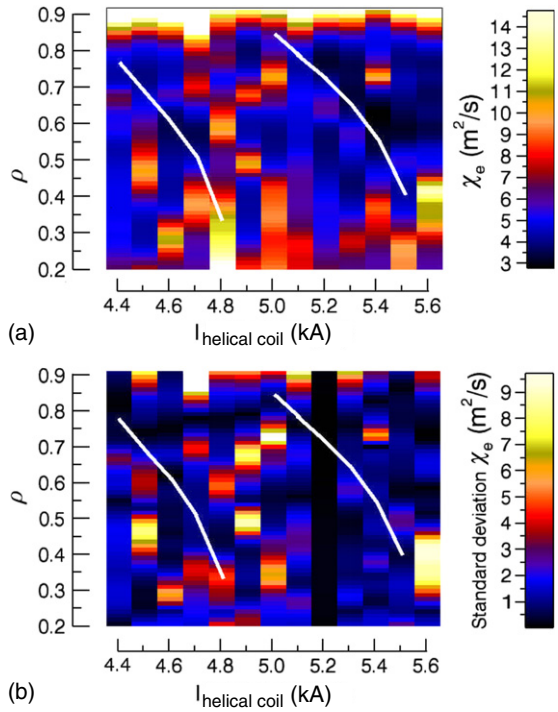

Figure 7. (*a*) Profiles of χ_e ($0.2 \leqslant \rho \leqslant 0.9$) as a function of helical coil current. The vacuum low order rationals $\iota = 8/5$ and $\iota = 5/3$ are shown with white lines. Values $\chi_e \geqslant 15\,\mathrm{m^2\,s^{-1}}$ are displayed in white. (*b*) Standard deviation values for the profiles of (*a*).

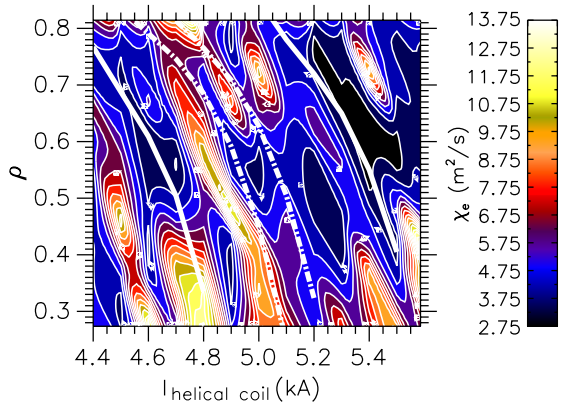

Figure 8. Same as figure 7(*a*) but after interpolating linearly the experimental data along a rotated mesh (see text). The path in vacuum of two higher order rationals ($\iota = 13/8$ and $\iota = 18/11$) is drawn with dashed lines.

they are, but also that lower order (maybe within the limited range of the figure) implies larger effect. In addition, this effect could be cooperative (note the comparatively small χ_e profile for $I_h \approx 5.2\,\mathrm{kA}$, where three low order rationals are plausibly present), something that is opposite to the common conception of deteriorated confinement due to the overlapping of stochastic zones.

Finally, it is worth noting that if this local effect of a low order rational of ι can be confirmed without any doubt, then the countour maps like figure 8 could be used reciprocally to identify the position of a certain value of ι to support, for example, calculations of the bootstrap current or other toroidal currents like those driven by microwaves. To give an example, let us hypothesize that the furrows in figure 8 do correspond to the suspected low order rationals so that, for instance, the 8/5 one follows the furrow up to $\rho = 0.3$ for $I_h \approx 4.9\,\mathrm{kA}$. Then we could conclude that the vacuum profile of the rotational transform is a good approximation up to $\rho \approx 0.5$, while for smaller ρ the vacuum rotational transform is *larger* than the one in the presence of the ECH plasma. In other words, there must be some net negative current integrated to the core region. To help in understanding this, the reader can take a typical ι-profile of the TJ-II (see figure 3), 'bend' it downwards for $\rho \lesssim 0.5$ and imagine how the thick white lines in figure 8 would look like under the scan in comparison with the vacuum values shown.

4.3. ECH power scan

In coincidence with other stellarators, χ_e in the TJ-II is found to increase with deposited heating power. Figure 9 shows the χ_e profiles averaged for each of the three different heating powers available labelled by the nominal values: 200 kW (dashed line),

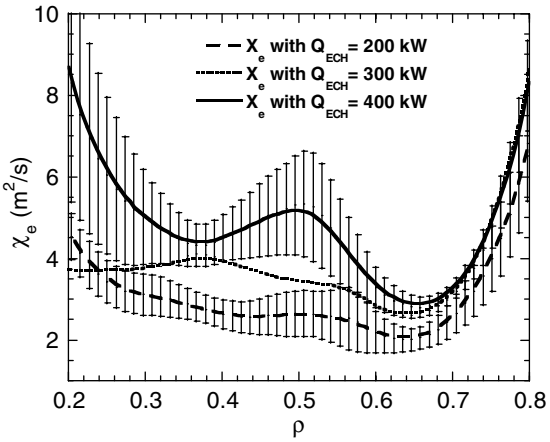

Figure 9. Thermal diffusivity profiles ($0.2 < \rho < 0.8$) for three different nominal ECH powers. The bars represent standard deviation.

300 kW (dotted line) and 400 kW (solid line). For the two extreme cases we also draw the standard deviation with vertical bars. These error bars are similar to the case with 300 kW but we do not draw them for clarity. The statistical dispersion is quite large, but the error bars suggest that in a large part of the plasma ($0.2 \lesssim \rho \lesssim 0.7$) the diffusivity does increase with heating power, most notably in the mid-radius. Outside $\rho \approx 0.7$ the diffusivities seem to be less affected by Q_{ECH}. A larger number of Q_{ECH} values with more discharges per heating power is needed to try significant fits to analytic forms of χ_e, at least for fixed radii as we did with the density scan. If we are to trust the values found on average, it looks like χ_e roughly doubles when Q_{ECH} increases from 200 to 400 kW in the bulk plasma. The 'peaking' of χ_e near $\rho = 0.5$ resembles what was found in our density scan and also in ECH power scans in the W7-AS stellarator [13], but before discussing this feature we need to clarify the possible role of low order rationals in altering the transport. Let us keep in mind at this point that the magnetic configuration here is the same as that of the density scan, while the average density is similar to the one in the rotational transform scan. Actually, the three scans share some discharges: those having a density around 0.65×10^{19} m^{-3} with a nominal power of 400 kW in the configuration with $I_h = 4.4$ kA. The power and density scans should be performed in different configurations to see what pertains to the ι profile and what can be explicitly related to the heating power or plasma density, respectively.

5. Summary

An interpretative analysis of transport in ECH plasmas of the TJ-II has been undertaken to (i) complement global scalings and (ii) to set the basis to elucidate the physical reasons for such scalings. χ_e depends locally on average electron density, rotational transform and ECH power deposited in the plasma.

In the density scan a reduction in χ_e, following a power-law $\chi_e(\rho) \propto \bar{n}^{\alpha(\rho)}$, is seen in the region where the density gradient occurs. This reduction reaches further inwards the larger the density and it is due to the increment in local densities while T_e remains unchanged. However, in the inner region ($\rho \lesssim 0.4$) the fits can be approximated by constant χ_e values due to statistical dispersion, which indicates a weak dependence on density. The large statistical deviation found in χ_e near $\rho = 0.5$ for the lowest densities decreases also as the density gets larger. In this respect, the study of the temporal variation of the electron temperature gradient in this region indicates that such variations do not determine the variability of χ_e. Rather, a comparison of TS profiles with similar densities suggests that the highly structured TS profiles provoke the variability of the smoothed profiles near $\rho = 0.5$ for the configuration that corresponds to this density scan (a common one for ECH operation of the TJ-II). Actually, in [23] it was found that the structures of TS profiles are less pronounced as the collisionality increases, which clearly agrees with our results. The fact that this region of high dispersion coincides with the position of the typical 'shoulder' observed in ECH density profiles is likely to be just a coincidence for this particular configuration.

A power-law dependence of the form $\chi_e(\rho) \propto \iota^{\beta(\rho)}$ with negative β was also suited for the rotational transform scan in the density gradient region, in agreement with the beneficial effect of the edge ι on confinement known from global scalings. However, reduced χ_e are found in all the studied plasma region where low order rotational surfaces are present independently of whether there is a significant power-law dependence. This effect can be seen with confidence in the outer half of the plasma, where the position of the low order rational must be pretty close to the vacuum one. Such a position can be defined with accuracy given the operational capabilities of the TJ-II: a fine scan in the currents of the central and helical conductors has allowed moving the $\iota = 8/5$ and $\iota = 5/3$ rationals through the plasma in a series of stationary discharges with the same volume and magnetic ripple. χ_e is found to be comparatively smaller in regions around the vacuum location of the low order rational. Moreover, it is suggested that the location of a low order rational can be indeed tracked after its effect in χ_e through the plasma. Thus, the effect of reduced χ_e following the path of the low order rational through the plasma can be followed all over the analysed region. To stress this we performed a linear interpolation of the experimental data guided by the path of the low order rationals in the ρ–I_h plane. The smaller values of χ_e go with the resonances $\iota = 8/5$ and $\iota = 5/3$ whilst the larger values of χ_e seem to configure in different 'ridges' flanking low order rational surfaces. For these ECH discharges, the experiments demonstrate a significant effect of the magnetic topology on χ_e or, in more general terms, on the electron temperature gradients. This should be distinguished from the so called core electron root confinement [30]. Such a phenomenon, as its name indicates, happens in the core plasma and it is linked to the establishment of a strong positive radial electric field. Particularly, data from the TJ-II device show that the improved electron heat confinement and the establishment of a large plasma potential $\sim \nabla T_e/e$ [31] is accompanied by a reduction of the core density [32]. Thus, a clear relationship is found between ECH and plasma potential. The presence of low order rationals in the core region can help in making the plasma system jump to the electron root solution for ambipolar fluxes or, simply, in accentuating the positive radial electric field. In our results we find a topological effect, not a transition phenomenon: firstly, we observe the *stationary* effect of low order rationals *everywhere* in the plasma although

we only present results where the effect is statistically more significative; second, a strong ECH power density is not necessary (it is negligible, rather) in our observations. Finally, and as far as we have checked, the density is not affected in the present case. A possible coincidence with the CERC phenomenon is that the structural change in transport may be linked to the radial electric field as it is modified (although we would think of its shear, not particularly its sign) by the presence of the magnetic resonance, e.g. via Reynolds stress driven poloidal flows. Since this only intends to be an informative work on experimental findings, we leave a longer discussion for a future work.

The dependence of χ_e on the ECH power deposited in the plasma shows a tendency to increase with heating power, especially in the region $\rho < 0.7$. The diffusivities approximately double when the ECH power is nominally increased from 200 to 400 kW in the inner zone of the plasma. A flatter χ_e profile, which tends to increase significantly near $\rho = 0.5$, is obtained for lower ECH power. Recalling that the configuration used for the ECH scan is the same as the one for the density scan, the results obtained prevent us from drawing conclusions about where in the plasma the peaking in χ_e takes place, since the results of the configuration scans present low order rationals as the main factors that influence the temperature gradient profile and, consequently, χ_e according to a diffusive description of transport.

The data compiled for this work have been considered sufficient to prove some main tendencies of ECH plasmas of the TJ-II stellarator. The density and ECH power scans have been found to generally agree with what is known from other devices. Very likely, the influence of the low order rationals on heat transport is not a distinct feature of the TJ-II but can be extended to, at least, low magnetic shear machines. It is, however, worth mentioning here that in a larger shear machine, the LHD Heliotron, a smaller transport *inside* an imposed island (low order rational) is also found [33]. Therefore, the results from the rotational transform scan might be a clear indication that there are physics phenomena to be taken into account in relation to the rotational transform profile. This could be important in the design of new stellarator devices. New experiments are being planned to deepen the relation between transport and magnetic resonances by measuring the plasma potential and, in the accessible outer region, fluctuation levels and flows. In addition, the possibility that the magnetic configuration affects transport must be checked also in neutral beam heated plasmas.

Acknowledgments

Amongst the members of the TJ-II Team we would like to thank Drs T. Estrada (reflectometry system), M. Ochando (bolometry) and A. López-Fraguas (magnetic configuration reconstruction).

References

[1] Yamada H. *et al* 2005 *Nucl. Fusion* **45** 1684
[2] Obiki T. *et al* 1989 Recent experiments on Heliotron E *Proc. 12th Int. Conf. on Plasma Physics and Controlled Nuclear Fusion Research 1988 (Nice, October 1988)* vol 2 (Vienna: IAEA) p 337
[3] Akulina D.K. *et al* 1989 Electron cyclotron heating of currentless plasma by an ordinary wave in the l-2 stellarator, *Proc. 12th. Int. Conf. on Plasma Physics and Controlled Nuclear Fusion Research 1988 (Nice, October 1988)* vol 2 (Vienna: IAEA) p 359
[4] Murakami M. *et al* 1991 Energy confinement and bootstrap current studies in the Advanced Toroidal Facility *Proc. 13th. Int. Conf. on Plasma Physics and Controlled Nuclear Fusion Research 1990 (Washington, DC, October 1990)* vol 2 (Vienna: IAEA) p 455
[5] Ascasíbar E. *et al* 2005 *Nucl. Fusion* **45** 276
[6] Brakel R. and W7-AS Team 2002 *Nucl. Fusion* **42** 903
[7] Renner H. *et al* 1991 Confinement properties of the 'advanced stellarator' Wendelstein W VII-AS, *Proc. 13th. Int. Conf. on Plasma Physics and Controlled Nuclear Fusion Research 1990 (Washington, DC, October 1990)* vol 2 (Vienna: IAEA) p 439
[8] Obiki T. *et al* 1991 Confinement improvement in ECH and NBI heated Heliotron E plasmas *Proc. 13th. Int. Conf. on Plasma Physics and Controlled Nuclear Fusion Research 1990 (Washington, DC, October 1990)* vol 2 (Vienna: IAEA) p 425
[9] López-Bruna D. *et al* 2006 Magnetic shear and transport in ECRH discharges of the TJ-II under ohmic induction *Technical Report* 1089 (Madrid, Spain: Ciemat)
[10] Okamura S. *et al* 1999 *Nucl. Fusion* **39** 1337
[11] Yamada H. *et al* 1994 *Nucl. Fusion* **34** 641
[12] Yamazaki K. *et al* 1992 *Nucl. Fusion* **32** 633
[13] Ringler H. *et al* 1990 *Plasma Phys. Control. Fusion* **32** 933
[14] Stroth U. *et al* 1998 *Plasma Phys. Control. Fusion* **40** 9
[15] Alejaldre C. *et al* 1999 *Plasma Phys. Control. Fusion* **41** A539
[16] Tabarés F.L. *et al* 2003 *J. Nucl. Mater.* **313–316** 839
[17] Herranz J. *et al* 2003 *Fusion Eng. Des.* **65** 525
[18] de la Luna E. *et al* 2001 *Rev. Sci. Instrum.* **72** 379
[19] Fontdecaba J.M. *et al* 2003 Charge exchange neutral particle analyser in TJ-II *Technical Report* 1014 (Madrid, Spain: Ciemat)
[20] Ochando M.A. *et al* 1999 *Rev. Sci. Instrum.* **70** 384
[21] Estrada T. *et al* 2001 *Plasma Phys. Control. Fusion* **43** 1535
[22] van Milligen B.Ph. *et al* 2003 *Rev. Sci. Instrum.* **74** 3998
[23] Herranz J. *et al* 2000 *Phys. Rev. Lett.* **85** 4715
[24] Balbín R. *et al* 2005 Ion temperature profiles during NBI plasma heating on the TJ-II stellarator *Proc. 15th Stellarator Workshop (Madrid, 2005)*
[25] Eguilior S. *et al* 2003 *Plasma Phys. Control. Fusion* **45** 105
[26] Fernández A. *et al* 2001 *Int. J. Infrared Millim. Waves* **22** 649
[27] Pereverzev G.V. and Yushmanov P.N. 2002 Astra automated system for transport analysis *Technical Report* IPP 5/98 (Garching: Max Plank Institut für Plasmaphysik)
[28] Ochando M.A. *et al* 2003 *Plasma Phys. Control. Fusion* **45** 221
[29] Vargas V.I. *et al* 2006 Difusión térmica electrónica experimental en plasmas ECRH del TJ-II *Technical Report* 1079 (Madrid, Spain: Ciemat)
[30] Yokoyama M. *et al* 2006 *Fusion Sci. Technol.* **50** 327
[31] Castejón F. *et al* 2004 *Nucl. Fusion* **44** 593
[32] Estrada T. *et al* 2006 *Fusion Sci. Technol.* **50** 127
[33] Ida K. *et al* 2004 *Nucl. Fusion* **44** 290